Optics Letters

Enhancing THz emission from nonlinear metasurfaces by a Bragg perfect absorber

EVIATAR MINERBI,[1,2,*] SYMEON SIDERIS,[2,3] AND TAL ELLENBOGEN[2,3]

[1] Raymond and Beverly Sackler Faculty of Exact Sciences, School of Physics and Astronomy, Tel-Aviv University, Tel-Aviv 6779801, Israel
[2] Center for Light-Matter Interaction, Tel-Aviv University, Tel-Aviv 6779801, Israel
[3] Department of Physical Electronics, School of Electrical Engineering, Tel-Aviv University, Tel Aviv, 6997801, Israel
*minerbi@mail.tau.ac.il

Received 20 March 2023; revised 4 May 2023; accepted 4 May 2023; posted 4 May 2023; published 18 May 2023

Nonlinear plasmonic metasurfaces were demonstrated recently as ultracompact tetrahertz (THz) sources, emitting relatively strong single-cycle THz pulses after femtosecond laser illumination. There has been great progress in their ability to generate controlled THz wavepackets; however, their overall emission strength has not yet been optimized. Here we numerically show that by designing a Bragg assisted perfect absorber we can improve the coupling of the pumping laser to the nonlinear metasurface. This results in over an order of magnitude enhancement of the THz signal. Moreover, we show that this method can be combined with other independent optimization schemes to further enhance the radiated THz, reaching over two orders of magnitude emission enhancement compared with previously studied plasmonic metasurfaces.

https://doi.org/10.1364/OL.489887

Over the past decades, the terahertz (THz) spectral regime, ranging from approximately 0.1 to 10 THz has been at the focus of active research that has led to a variety of emerging applications. Numerous studies show the potential of THz waves in a wide variety of areas such as fast wireless communication [1,2], non-destructive imaging of optically opaque materials [3,4], nonionizing biomedical tomography [5,6], molecular spectroscopy [7], and material science [8,9]. The further progress of these ever-growing THz technologies requires efficient and compact broadband emitters and detectors.

In recent years, there has been rapid progress in the development of tabletop THz sources generating broadband THz pulses, including photoconductive antennas (PCAs) [10] and optical rectification (OR) in nonlinear media [11,12]. However, these generation schemes typically require either external electrical wiring or phase-matching schemes, and are very limited in their ability to control the emitted THz pulses. One way to circumvent these drawbacks is to use nonlinear metasurfaces [13,14,15]. Recently, it was shown that exciting plasmonic metasurfaces with a near infrared (NIR) femtosecond laser results in THz emission, comparable to that emitted from an orders of magnitude thicker zinc telluride (ZnTe) nonlinear crystal [16,17,18]. Following these observations, metasurfaces allowing local phase control for generation of spatiotemporally tailored THz wavepackets were designed [18]. These results were quickly followed by demonstrations of a variety of binary phase, and full phase-gradient, functional metasurface emitters [19,20,21,22]. It was found that the relatively strong THz emission is due to the presence of a thin indium tin oxide (ITO) film, and the enhancement originates from the large optical nonlinearities of ITO at excitation wavelengths where the permittivity is near zero, in addition to further field confinement [21,23]. However, although these metasurfaces exhibit extremely high conversion efficiencies compared to their thickness, their overall maximal optical to THz conversion efficiency is still relatively low, of the order of 10^{-6} [24]. Therefore, there is a strong interest to further increase their conversion efficiencies to make them more viable for applications. One direction that was theoretically proposed to achieve this goal was to use a dark mode to increase the absorption and optimize the light–matter interaction [25]. However, the structure suggested in [25] requires a challenging fabrication process and does not account for the ITO layer which was shown to be crucial for the THz emission [21,23].

Here, we theoretically and numerically investigate a simple fabrication design based on a distributed Bragg perfect absorber configuration to enhance the THz emission by maximizing the absorption and the interaction with the metasurface.

We start by examining a typical metasurface comprised of gold split ring resonators (SRRs) on an ITO coated glass substrate [Fig. 1(a)], as was used in various previous works demonstrating THz generation [16,18,19,23,24]. In this design, the arms and base of the SRRs are 200 nm long, they are arranged in a square lattice with a periodicity of 400 nm, and the thicknesses of the gold and ITO layer are 40 nm and 20 nm, respectively. We investigate the optical linear performance of the metasurface by using a 3D full wave finite-element method software (COMSOL Multiphysics) and apply periodic boundary conditions to the unit cell. The optical properties of the ITO layer were obtained by considering a Drude permittivity, and the fitting parameters were taken from [23]. All other material parameters were taken from the software's libraries.

In Fig. 1(b), we plot the linear response of the metasurface when pumped with light polarized along the base of the SRRs (x-polarization) at normal incidence. It can be seen that the transmission spectra through the metasurface has two dips at $\lambda = 1200$ nm and $\lambda = 1500$ nm. As mentioned in previous studies, these dips correspond to the resonance of the coupled SRR–ITO system [21,23]. Looking at the absorption of the metasurface,

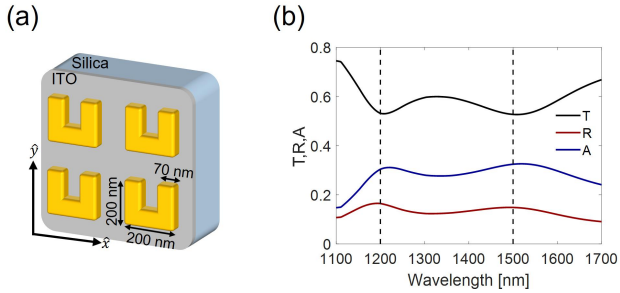

Fig. 1. Metasurface characteristics. (a) Illustration along with the dimensions of the SRRs comprising the metasurface. (b) Linear response spectrum when the metasurface is illuminated at normal incidence and polarized along x. T, transmission (black line); R, reflection (red line); A, absorption (blue line).

we notice that only up to 30% of the pump field is absorbed, which may indicate that the light–matter interaction is far from optimal.

To overcome this issue and to maximize the absorption, we introduce a Bragg absorber meta-structure (BAMS) in Fig. 2(a). This structure consists of gold SRRs on a thin ITO film on top of alternating layers of silica and silicon which possess large refractive index contrast in the NIR regime, together with relatively low losses for THz frequencies, and are easy to fabricate. The thickness of each layer (silica/silicon) is calculated so that it will fulfill the Bragg condition [26], namely:

$$d = \lambda/4n_{SiO_2,Si}(\lambda), \tag{1}$$

where λ is the wavelength and $n_{SiO_2,Si}(\lambda)$ is the refractive index of the layer. We start by looking at the resonance of the metasurface at $\lambda = 1500$ nm [Fig. 1(b)] and design the thicknesses of the BAMS layers accordingly. The absorption as a function of number of layers and wavelength for this design is presented in Fig. 2(b). As expected, the broadband absorption increases with the number of layers, and is maximized for the designed wavelength. In Fig. 2(c), we plot the absorption, along with the transmission and reflection at $\lambda = 1500$ nm as a function of the thickness of the entire stack. For thicknesses above ~1.1 μm (corresponding to 6 layers), the absorption starts to saturate, reaching near perfect absorption. Since our goal is to achieve maximal absorption using the thinnest structure possible, we design our BAMS with 6 layers throughout the manuscript. In this configuration, over 95% of the pump light is absorbed in the structure and the rest is mainly transmitted [see Fig. 2(c)].

The THz generation by plasmonic metasurfaces on ITO is dominated by a second-order nonlinear process [16,23], and hence $I_{THz} \propto (\epsilon_0 \chi^{(2)}_{eff} E_{pump} E^*_{pump})^2 \propto |E_{pump}|^4$. Therefore, we can estimate the THz field enhancement by examining the field confinement by the nanoparticles and the ITO layer at excitation NIR wavelengths. The local field at varying pumping wavelengths, along with the field enhancement compared with a control metasurface on an ITO coated glass [Fig. 1(a)] is shown in Fig. 2(d). The BAMS design enhances the local linear fields in the SRR–ITO region, which is responsible for the THz emission, by ~1.8 times compared with the control, thus predicting an order of magnitude enhanced THz emission.

After investigating the linear response of the system, we examine the nonlinear interaction. To model the THz generation, we consider the hydrodynamic model which treats the free electrons

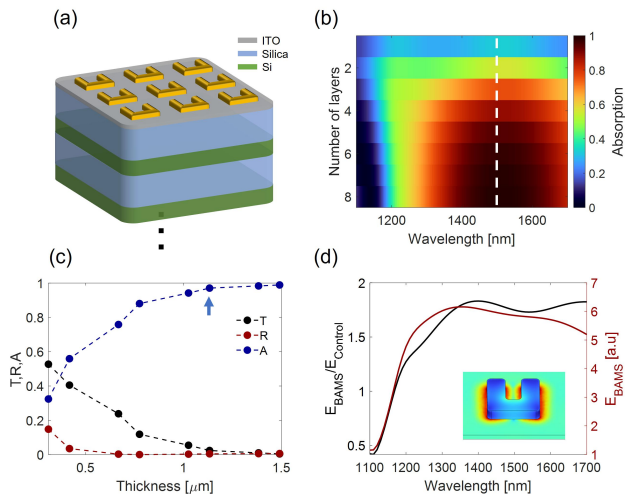

Fig. 2. (a) Illustration of the Bragg absorber meta-structure, comprised of SRRs on a thin ITO layer and alternating silica and silicon layers. (b) Absorption as a function of number of layers and pumping wavelength. Dashed line marks the designed wavelength at 1500 nm. (c) Linear response of the structure for a pumping wavelength of 1500 nm as a function of the stack thickness. T, transmission (black); R, reflection (red); A, absorption (blue). Arrow indicates the optimal structure between absorption and thickness. (d) Integrated electric field for the BAMS (red) and field enhancement compared with a control metasurface (black) as a function of pumping wavelength. Inset shows normalized electric field at $\lambda = 1500$ nm (log scale) over the integrated area on the nanoparticle and the ITO layer.

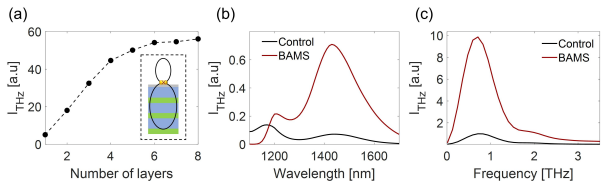

Fig. 3. Nonlinear emission from the BAMS. (a) Generated THz radiation as a function of the number of layers in the BAMS. Inset shows a schematic of the THz radiation pattern from the BAMS. (b) THz intensity as a function of pumping wavelength for the control metasurface (black) and for the BAMS (red). (c) Calculated emission spectrum from the control (black) and the BAMS (red) when pumping at $\lambda_{Pump} = 1430$ nm.

in the metal and ITO as an electron gas that obeys Euler's equation [27,28,29].

Following previous studies [23,30], the nonlinear currents which act as the source for the THz generation are modeled as

$$\vec{J}_{nl} = \frac{-i}{eN_0}[\omega_2(\nabla\cdot\vec{P}_1)\vec{P}^*_2 - \omega_1(\nabla\cdot\vec{P}^*_2)\vec{P}_1 + \frac{\omega_1\omega_2}{\omega_3 + i\Gamma}((\vec{P}_1\cdot\nabla)\vec{P}^*_2 + (\vec{P}^*_2\cdot\nabla)\vec{P}_1], \tag{2}$$

where $\vec{P}_{1,2}$ is the polarization at frequency $\omega_{1,2}$ and $\omega_3 = \omega_2 - \omega_1$. Here, N_0 and e are the electron density and charge, respectively, and Γ is the total electron collision rate. Using this model, we plot in Fig. 3(a) the THz field as a function of the number of layers in the BAMS. The enhancement of the radiated THz saturates after 6 layers, where the absorption saturates as well, confirming that the 6-layer BAMS is optimized. We note that the

dipole emission from the SRRs is stronger toward the dielectric side [inset of Fig. 3(a)]; however, the THz emission that radiates through the meta-structure is highly dependent on the specific film characteristics, their optical properties at THz frequencies, and the substrate. Therefore, for simplicity, we consider the THz emitted to the air side in the reflection configuration. We compare the THz generated from the BAMS with the control in Figs. 3(b) and 3(c). The optimal enhancement is obtained near the designed operation wavelength at $\lambda_{Pump} = 1430$ nm. In addition, the THz field is also enhanced for a broad range of pumping wavelengths, due to the large refractive index contrast. Finally, in Fig. 3(c), we plot the THz emission spectra following illumination with $\lambda_{Pump} = 1430$ nm, showing that the BAMS does not affect the broadband spectrum of the radiated THz field, only increases its intensity.

After showing that our simplistic design works as expected, we study the BAMS configuration more systematically, and carefully design it to optimize the generation efficiency. We do so by sweeping over the parameter space of our design and varying the thickness of the layers composing the BAMS according to Eq. (1). In Fig. 4(a), we plot the absorption as a function of the BAMS designed wavelength (λ_{BAMS}) and the pumping wavelength. By designing the structure to overlap with the resonance of the system, the absorption is maximized, reaching almost 100%. The generated THz field is shown in Fig. 4(b), and the maximal signal is obtained for $\lambda_{BAMS} = 1200$ nm and $\lambda_{Pump} = 1150$ nm. The THz field does not exactly follow the absorption of the system since it originates from the more complex nonlinear current which depends on the spatial distribution of the polarization [Eq. (2)]. Near the ENZ wavelength of the ITO layer ($\lambda_{ENZ} = 1245$ nm), the electric field, and thereby the polarization, is highly enhanced. Therefore, higher THz generation is expected when pumping at shorter wavelengths [Fig. 4(b)].

Next, we incorporate the THz generation dependence on the pumping power. It was experimentally observed that the THz signal generated from plasmonic metasurfaces on ITO saturates

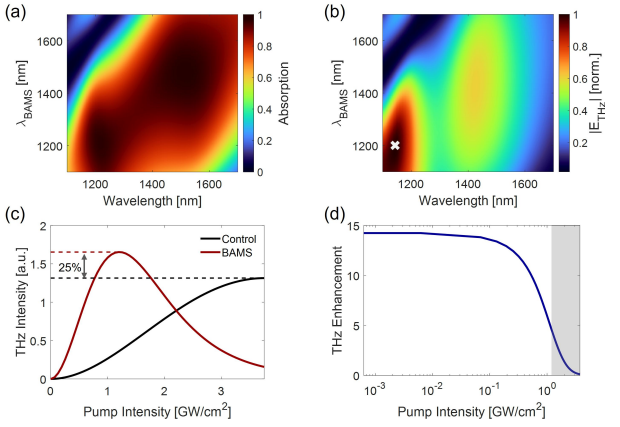

Fig. 4. Complete analysis of the BAMS design. (a) Absorption of the BAMS as a function of designed wavelength and pumping wavelength. (b) Generated THz radiation (normalized) as a function of designed wavelength and pumping wavelength. The X sign marks the optimized design. (c) Intensity of THz signal as a function of pump fluence accounting for temporal dynamics, for the control (black) and BAMS (red). (d) THz enhancement of the BAMS compared with the control as a function of pump fluence. Shaded area marks the region above saturation of the BAMS.

at increasing pumping powers [23,24,31]. This behavior was explained by temporal dynamics which play a significant role at high powers [23]. We follow the model proposed in [23] and incorporate it in our study to account for these dynamics. In this model, the femtosecond pumping pulse acts as an energy source that gives rise to hot electron dynamics, which alter the optical response of the system and shift the ENZ point, thus modifying the nanoparticle–ITO coupling at a sub-picosecond time scale. As a result, the THz intensity saturates at high pumping powers. The dynamics are inherently dependent on the absorption of the system, therefore, increasing the absorption results in higher temperatures at lower pumping powers. Hence, for the BAMS, the maximal THz radiation value occurs for much lower pumping intensities [Fig. 4(c)]. Up to the peak generated THz intensity, the BAMS structure significantly enhances the emission, allowing to drive the metasurface at lower excitation intensities. In addition, the peak intensity of the optimal BAMS is ~25% stronger than the peak intensity of the control. Plotting the ratio of the generated THz from the BAMS and the control as a function of pumping pulse intensity [Fig. 4(d)] shows that the maximal 14-fold enhancement is obtained for low pumping intensities. As the pump power is increased however, the overall enhancement is reduced, reaching 5-fold enhancement at the peak THz intensity of the BAMS (pump intensity of 1.2 GW/cm^2). Therefore, the proposed scheme is optimized for low-power pumping lasers such as optical parametric oscillators [32]. The immediate benefit from this finding is that it is well suited for the need of efficient, low cost, and compact THz sources without requiring large and expensive pumping lasers.

Finally, we show that the proposed structure can be integrated with additional enhancement schemes to increase the optical to THz conversion efficiency further. As an example, a method to improve the THz radiation efficiency from the plasmonic metasurfaces by structuring the ITO was very recently demonstrated [24]. It was shown that while the ITO film is crucial for the enhancement of the THz generation [21,23], its conductive nature at low frequencies truncates the generated signal that propagates to the far field [24]. Therefore, by etching the ITO around the meta-atoms, it is still possible to harness the enhanced fields from the remaining ITO and improve the radiation efficiency. This simple yet very effective method resulted in an order of magnitude enhancement in the measured THz signal. Here, we investigate the combination of these two independent conversion efficiency enhancement schemes. Figure 5(a) shows the schematic design combining the multi-physical approach to both optimize the nonlinear interaction by using BAMS and effectively radiate the THz waves by etching the ITO. In Fig. 5(b), we compare the emission spectra from the control metasurface, the BAMS, and etched BAMS (optimized). Our simulations show that the etched BAMS results in over

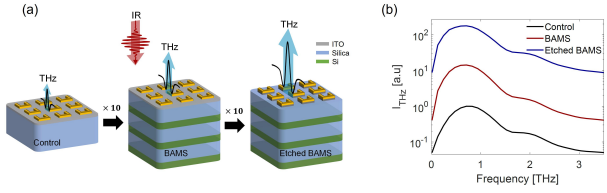

Fig. 5. (a) Illustration of the meta-structures under consideration and their THz emission. (b) THz intensity spectra for the control (black), BAMS (red), and etched BAMS (blue).

2 orders of magnitude enhancement compared with the control metasurface. The scheme proposed in this Letter can also be applied to enhance the emission of all dielectric metasurfaces which were recently shown to generate THz radiation as well [33,34].

In conclusion, we showed that typical plasmonic metasurfaces are not optimized for THz generation since they do not fully exploit the pump energy. To overcome this, we introduce a BAMS scheme which is designed to match the hybrid resonance of the strongly coupled SRR–ITO system. We show that in this configuration, perfect absorption can be achieved, and the field is highly concentrated on the metasurface. Analyzing the THz emission from such a device reveals up to 14-fold enhancement compared with the control metasurface at low pumping powers, in addition to ∼25% enhanced peak intensity at much lower pumping powers. Furthermore, we show that this method can be combined with other enhancement schemes to obtain even higher efficiencies. Specifically, we show that another order of magnitude enhancement can be gained by etching the ITO, thus leading to a total enhancement of over two orders of magnitude. According to previous experimental observations, the conversion efficiency from the control metasurface was comparable to a thick ZnTe crystal and was estimated to be $\sim 9 \times 10^{-8}$ [18,11]. PCAs, however, showed much higher efficiencies and therefore were more attractive despite their drawbacks. Our demonstrated multiphysics design enhances the radiated THz by over an order of magnitude, while requiring reduced pumping powers. Therefore, the theoretically estimated conversion efficiency reaches 4×10^{-6}, placing plasmonic metasurfaces above thick inorganic crystals and alongside photoconductive antennas [35] in terms of conversion efficiencies. This work motivates additional studies that can be integrated together to further enhance the THz radiation, thus paving the way toward more efficient, ultracompact, and fully integrated THz sources.

Funding. H2020 European Research Council (715362).

Disclosures. The authors declare no conflicts of interest.

Data availability. Data underlying the results presented in this paper are not publicly available at this time but may be obtained from the authors upon reasonable request.

REFERENCES

1. T. Nagatsuma, G. Ducournau, and C. C. Renaud, Nat. Photonics **10**, 371 (2016).
2. H. Elayan, O. Amin, R. M. Shubair, and M.-S. Alouini, in *2018 International Conference on Advanced Communication Technologies and Networking (CommNet)* (2018), pp. 1–5.
3. S. Zhong, Front. Mech. Eng. **14**, 273 (2019).
4. E. Castro-Camus, M. Koch, and D. M. Mittleman, Appl. Phys. B **128**, 12 (2022).
5. X. Yang, X. Zhao, K. Yang, Y. Liu, Y. Liu, W. Fu, and Y. Luo, Trends Biotechnol. **34**, 810 (2016).
6. L. Yu, L. Hao, T. Meiqiong, H. Jiaoqi, L. Wei, D. Jinying, C. Xueping, F. Weiling, and Z. Yang, RSC Adv. **9**, 9354 (2019).
7. X. Fu, Y. Liu, Q. Chen, Y. Fu, and T. J. Cui, Front. Phys. **10**, 1 (2022).
8. P. Salén, M. Basini, S. Bonetti, J. Hebling, M. Krasilnikov, A. Y. Nikitin, G. Shamuilov, Z. Tibai, V. Zhaunerchyk, and V. Goryashko, Phys. Rep. **836-837**, 1 (2019).
9. P. Bowlan, J. Bowlan, S. A. Trugman, R. Valdés Aguilar, J. Qi, X. Liu, J. Furdyna, M. Dobrowolska, A. J. Taylor, D. A. Yarotski, and R. P. Prasankumar, Optica **4**, 383 (2017).
10. N. M. Burford and M. O. El-Shenawee, Opt. Eng. **56**, 010901 (2017).
11. F. Blanchard, L. Razzari, H. C. Bandulet, G. Sharma, R. Morandotti, J. C. Kieffer, T. Ozaki, M. Reid, H. F. Tiedje, H. K. Haugen, and F. A. Hegmann, Opt. Express **15**, 13212 (2007).
12. L. Guiramand, J. E. Nkeck, X. Ropagnol, T. Ozaki, and F. Blanchard, Photonics Res. **10**, 340 (2022).
13. E. Rahimi and R. Gordon, Adv. Opt. Mater. **6**, 1800274 (2018).
14. A. Krasnok, M. Tymchenko, and A. Alù, Mater. Today **21**, 8 (2018).
15. S. Keren-Zur, L. Michaeli, H. Suchowski, and T. Ellenbogen, Adv. Opt. Photonics **10**, 309 (2018).
16. L. Luo, I. Chatzakis, J. Wang, F. B. P. Niesler, M. Wegener, T. Koschny, and C. M. Soukoulis, Nat. Commun. **5**, 3055 (2014).
17. D. K. Polyushkin, E. Hendry, E. K. Stone, and W. L. Barnes, Nano Lett. **11**, 4718 (2011).
18. S. Keren-Zur, M. Tal, S. Fleischer, D. M. Mittleman, and T. Ellenbogen, Nat. Commun. **10**, 1778 (2019).
19. E. Minerbi, S. Keren-Zur, and T. Ellenbogen, Nano Lett. **19**, 6072 (2019).
20. C. McDonnell, J. Deng, S. Sideris, T. Ellenbogen, and G. Li, Nat. Commun. **12**, 30 (2021).
21. Y. Lu, X. Feng, Q. Wang, X. Zhang, M. Fang, W. E. I. Sha, Z. Huang, Q. Xu, L. Niu, X. Chen, C. Ouyang, Y. Yang, X. Zhang, E. Plum, S. Zhang, J. Han, and W. Zhang, Nano Lett. **21**, 7699 (2021).
22. C. McDonnell, J. Deng, S. Sideris, G. Li, and T. Ellenbogen, Nano Lett. **22**, 2603 (2022).
23. E. Minerbi, S. Sideris, J. B. Khurgin, and T. Ellenbogen, Nano Lett. **22**, 6194 (2022).
24. S. Sideris, E. Minerbi, C. McDonnell, and T. Ellenbogen, ACS Photonics **9**, 3981 (2022).
25. M. Fang, N.-H. Shen, W. E. I. Sha, Z. Huang, T. Koschny, and C. M. Soukoulis, Phys. Rev. Lett. **122**, 027401 (2019).
26. B. Gao, J. P. George, J. Beeckman, and K. Neyts, Opt. Express **28**, 12837 (2020).
27. C. Ciracì, E. Poutrina, M. Scalora, and D. R. Smith, Phys. Rev. B **85**, 201403 (2012).
28. M. Fang, K. Niu, Z. Huang, W. E. I. Sha, X. Wu, T. Koschny, and C. M. Soukoulis, Opt. Express **26**, 14241 (2018).
29. M. Fang, Z. Huang, W. E. I. Sha, and X. Wu, IEEE J. Multiscale Multiphysics Comput. Tech. **2**, 194 (2017).
30. S. Sideris and T. Ellenbogen, Opt. Lett. **44**, 3590 (2019).
31. W. Jia, M. Liu, Y. Lu, X. Feng, Q. Wang, X. Zhang, Y. Ni, F. Hu, M. Gong, X. Xu, Y. Huang, W. Zhang, Y. Yang, and J. Han, Light: Sci. Appl. **10**, 11 (2021).
32. M. Tal, S. Keren-Zur, and T. Ellenbogen, ACS Photonics **7**, 3286 (2020).
33. Y. Tu, X. Sun, H. Wu, X. Zan, Y. Yang, N. Liu, X. Wang, C. Meng, Z. Lyu, Z. Zhu, K. Liu, D. Zhang, and Z. Zhao, Front. Phys. **10**, 1 (2022).
34. H. Jung, L. L. Hale, S. D. Gennaro, J. Briscoe, P. P. Iyer, C. F. Doiron, C. T. Harris, T. S. Luk, S. J. Addamane, J. L. Reno, I. Brener, and O. Mitrofanov, Nano Lett. **22**, 9077 (2022).
35. I. A. Glinskiy, R. A. Khabibullin, and D. S. Ponomarev, Russ. Microelectron. **46**, 408 (2017).